Calculation of the output power in self-amplified spontaneous radiation using scaling of power with number of simulation particles

Li Hua Yu
National Synchrotron Light Source, Brookhaven National Laboratory, Upton, New York 11973
(Received 10 December 1997; revised manuscript received 1 July 1998)

Recent advances in self-amplified spontaneous emission (SASE) experiments stimulate interest in quantitative comparison of measurements with theory. In this paper we show that the widely used simulation code TDA3D, developed by Tran and Wurtele [Comput. Phys. Commun. **54**, 263 (1989)] even though a single frequency code, can be used to determine the output power in the SASE process with excellent approximation in the exponential growth regime. The method applies when the gain is not very high, which is a special advantage, because when the gain is not very high, the analytical calculation is particularly difficult since the exponential growing term does not dominate. The analysis utilizes a scaling relation between the output power and the number of simulation particles in the code TDA3D: $\langle P\rangle = N'_\lambda/N_\lambda\langle P'\rangle$, where $\langle P\rangle$ is the output power and N_λ is the line density of the electrons, while $\langle P'\rangle$ is the calculated output power using a line density N'_λ of the number of simulation particles in the code TDA3D. Because of the scaling property, the number of simulation particles can be taken to be many orders of magnitude less than the actual experiment. Comparison of our results with experiment yields new insight into the SASE process. [S1063-651X(98)08110-0]

PACS number(s): 52.75.Ms

I. INTRODUCTION

Recently, there have been a number of experimental demonstrations of self-amplified spontaneous emission (SASE) [1]. All of them measured the SASE radiation pulse energy as a function of pulse charge, showing a deviation from linear dependence. A comparison of these results with simulation and analytical theory is urgently needed.

The theory on the average power, bandwidth, and transverse mode expansion for SASE was developed years ago [2–7]. A consistent one-dimensional (1D) SASE theory incorporating the equations of motion of the electrons and the Maxwell equations together and solving the initial value problem was derived in Refs. [4,5]. The theory was extended to a 3D case in Refs. [6,2]. In Ref. [2] the 3D problem for a parallel electron beam was explicitly solved so that it can be applied directly for a quantitative comparison with simulations. Also, a method was developed to investigate the transverse coherence of the output radiation, relating it to the degeneracy of the guided modes [2,3]. The theory was also formulated in a way allowing analysis of the problem with finite energy spread. In Ref. [3] the equivalent noise power was identified as the wiggler radiation in the first two power gain lengths. The shot noise formula was derived for beam sizes ranging from the large to the small beam size limits, and the coupling of shot noise into different guided modes was determined. Later, this result was extended to include the effect of the angular divergence of the electrons [7]. The theory [2,3] is appropriate for comparison with the recent experiment.

However, there are limitations on the applicability of the analytic theory, especially when the gain is not sufficiently high to assume that the exponentially growing terms dominate. Also, when the electron beam is not matched to the focusing of the wiggler, the electron beam size is not constant in the wiggler, as is the case for a recent 1 μm SASE experiment at the Accelerator Test Facility (ATF) at Brookhaven National Laboratory and several others, the analytic estimates are not accurate. Hence, a simulation is very useful in these cases. There are simulation codes taking into account broad bandwidth that can be used to simulate SASE, for example, the well known code GINGER [8]. These codes take much longer running time than the single frequency code TDA3D [12], developed by Tran and Wurtele. Hence, it would be very useful if one can use the familiar and relatively simpler code TDA3D to simulate the SASE process.

In this paper we shall show that the TDA3D code, which has been modified to include harmonic generation calculation, can be directly used for this purpose. One reason that this is possible is that in the linear regime there is a very simple scaling relation between the number of simulation particles and the output power. Hence, the number of simulation particles can be made much smaller than the actual number of electrons in the beam, making the simulation practical. In this paper we derive the scaling relation for a parallel electron beam, and then test it by simulation. We also found by simulation that for a beam with finite emittance, and even for an unmatched beam, the scaling relation is still valid. This indicates the general validity of the scaling. We shall show that although this method does not provide all the information for different aspects of the SASE process, it turns out to give an excellent approximation for the output power.

As a test, the ratio of the SASE radiation spectrum to the spontaneous radiation spectrum is calculated for an idealized parallel beam by both the analytical theory developed in Refs. [2,3] and the numerical methods developed here using the code TDA3D. These two very different methods agree with each other very well, strongly supporting their validity.

It is clear from this discussion that this method uses an entirely different approach to reduce the number of simulation particles as compared with the simulation codes such as GINGER. We shall briefly compare these two approaches.

As explained in Ref. [9], the codes such as GINGER use an artificial initial distribution to simulate the SASE start-up process. To suppress the increased shot noise due to the limited number of simulation particles, the codes are based on a distribution with equally spaced particles. To introduce a controlled noise, they generate a random deviation from the equally spaced distribution with a controlled rms value of the displacements. The rms displacement is chosen ''to reproduce the same mean and variance of the quantity'' [9] $\langle \exp(-i\theta)\rangle = (1/N)\,\Sigma_{j=1}^{N} \exp(-i\theta_j)$, where θ_j is the ponderomotive phase of the particle j, and N is the total number of electrons, ''using, instead of the real distribution and number N of electrons, an artificial distribution with a much smaller number n.'' While the mean and variance of the relevant quantity simulate the initial status of the system, it is not evident that the higher moments of this quantity would not affect the high gain process, it is also not evident that the mean and variance of the relevant quantity would remain to be the same as the realistic distribution during the high gain process, even though the simulations did show an agreement with the linear high gain theory.

As compared with these codes, our method uses a realistic distribution instead of an artificial evenly spaced distribution. We do not attempt to suppress the noise due to the limited number of simulation particles. Rather, we use the scaling relation to go from the simulation case with increased start-up noise (due to the reduced number of simulation particles) to the realistic case. In this manner, we obtain the correct radiation power in the linear regime. Another difference is that our method uses single frequency codes such as TDA3D, instead of the multifrequency or time-dependent codes to carry out the calculation, (the reason we can use a single frequency code to calculate for an intrinsically broadband SASE process will be explained in Sec. II). Our method does not require a modification to the single frequency codes, and hence can be used directly by anyone familiar with the code TDA3D. Because these codes are time independent, they need much shorter CPU time than the time-dependent codes.

There is a disadvantage associated with our method, i.e., it only applies to the linear regime, not the saturation regime. However, the fact that this method needs much shorter CPU time and that many people are more familiar with the single frequency codes such as TDA3D than with time-dependent codes makes our method a useful complementary approach to the problem.

In this paper we assume the electron bunch is sufficiently long and the bunch shape is sufficiently smooth, so the coherent spontaneous emission (CSE) from the detailed structure in the bunch of order of the radiation wavelength is negligible. In short, we discuss incoherent self-amplified spontaneous emission, starting from shout noise. In an actual experiment, one should use experimental technique to distinguish CSE and SASE. One example of the experimental method to rule out the existence of CSE is to show that in the experiment there is no enhancement to the transition radiation due to coherent transition radiation in the wavelength range of interest. If one can rule out the existence of the CSE in an experiment, the method developed here can then be applied.

In Sec. II, we first explain why a single frequency code can be used to calculate SASE power, which has intrinsically a finite bandwidth. Then we explain why the output power scales inversely with the number of simulation particles in the code TDA3D. Next, in Sec. III we describe an analytical estimate of the output power from a free-electron laser (FEL) with an idealized parallel electron beam with step-function transverse profile. Finally, in Sec. IV we present the comparison of the numerical and the analytical methods, then we apply the method to the practical case of the 1 μm SASE experiment at ATF of BNL.

II. THE SCALING RELATION AND THE NUMERICAL SIMULATION

First, we shall explain why a single frequency code TDA3D can be used to calculate the output power of SASE, a phenomenon with finite bandwidth. Later, we will show how one can use very few simulation particles to simulate the experiment with a huge number of electrons, by deriving a scaling relation between power and the number of simulation particles.

In the original TDA code, all the simulation particles are limited to within one optical wavelength, or one cell. During a later modification of the code for harmonic generation calculation [10], we extended the code such that the simulation particles could be in an arbitrary number of wavelengths. It is easy to see that if the number of cells is n_l, then the code is describing a fictitious electron-beam distribution with longitudinal periodic structure of n_l optical wavelengths. That is, we artificially set a periodic boundary condition on the electron beam with period equal to n_l optical wavelengths. In this case, the radiation spectrum has a line structure with frequency spacing ω_s/n_l, where ω_s is the optical frequency.

To illustrate this point we plot the power spectrum of spontaneous radiation in Fig. 1. When the distribution is nonperiodic, the spontaneous radiation spectrum from a wiggler with $N_w=10$ periods is a continuum as shown by Fig. 1(A), with a width of $\omega_s/N_w=\omega_s/10$. When we artificially introduce a fictitious periodic structure in the electron-beam distribution, the radiation has a line structure, as shown by Figs. 1(B)–1(D) for three different cases. The total power is the sum of the height of the lines. We denote the slippage distance by $l_s=N_w\lambda_s$, and the distribution period by $l=n_l\lambda_s$, then Fig. 1(B) corresponds to the case $l \gg l_s$, the line spacing ω_s/n_l is much narrower than the spontaneous radiation width ω_s/N_w, and the dense line structure gives a profile of the spontaneous spectrum of Fig. 1(A). Figure 1(C) is for a case where $l=2l_s$, and there are only two lines left. When we choose the period to be equal to the slippage distance $l=l_s$, i.e., when $n_l=N_w$, the line spacing is equal to the radiation spectrum width, and hence there is only one line, as shown in Fig. 1(D).

The code TDA3D, developed from TDA, only describes a monochromatic radiation beam, i.e., the Maxwell equation is reduced to describe a single frequency ω_s. To rigorously describe SASE, the code should be further modified to include other frequencies such as $\omega_s(n_l-1)/n_l$, $\omega_s(n_l+1)/n_l$, etc. Now, if we choose n_l to be equal to, or larger than, the number of periods N_w in the wiggler, the slippage $N_w\lambda_s$ is smaller than the spacing between the periodic boundaries of the electron beam. Hence there is no interac-

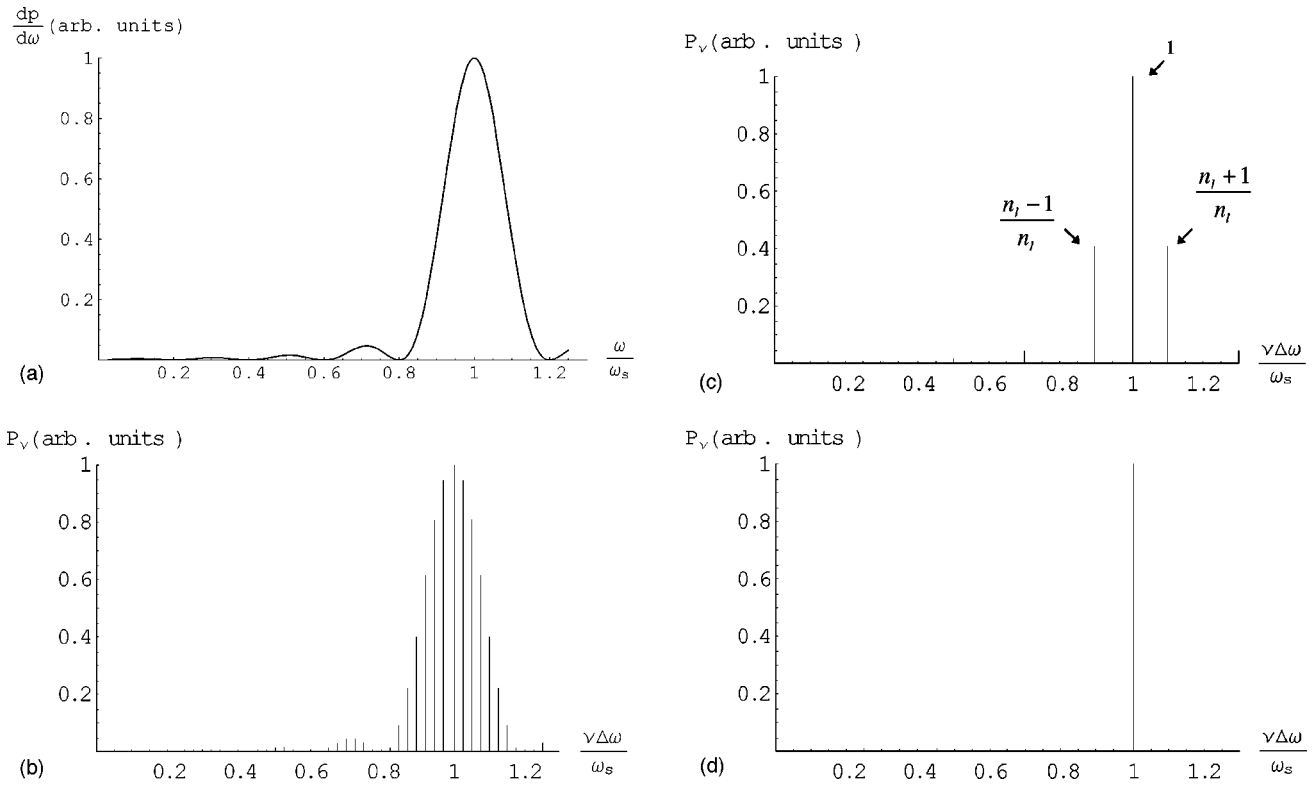

FIG. 1. (a) Illustration of the spontaneous power spectrum of a nonperiodic structures. (b) Line spectrum of a structure with period much longer than the slippage distance. In this case $dP/d\omega=\Sigma_{\nu=-\infty}^{\infty}P_\nu\delta(\omega-\nu\Delta\omega)$, where $\Delta\omega=\omega_s/n_l$. We plot P_ν vs $\nu\Delta\omega$ ($n_l\gg N_w$). (c) Distribution period l two times longer than the slippage distance l_s ($n_l=2N_w$). (d) Distribution period l equal to the slippage distance l_s ($n_l=N_w$).

tion between any two of the idealized periods of the electron distribution. If we combine the contributions from all the frequency lines, the calculated output energy within one idealized period of the electron distribution is the same as it would be from a nonperiodic structure in the electron beam, i.e., the same as for the realistic case for SASE process. The output power in one of the many lines is the power within a bandwidth of $1/N_w$ centered around that line, or more precisely, the power spectrum times the bandwidth ω/N_w: $(\omega_s/N_w)(d\rho/d\omega)$.

Now from the 1D analytic theory of SASE, we know that the rms bandwidth of the SASE spectrum is [4,5]

$$\frac{\sigma_\omega}{\omega}=\left(\frac{3\sqrt{2}\rho}{k_wL_w}\right)^{1/2}, \tag{1}$$

where ρ is the Pierce parameter [11], k_w the wiggler wave number, L_w the wiggler length. For convenience, we shall rewrite the width in terms of a ''full width,'' which is defined so that when it is multiplied by the peak power spectrum $dP/d\omega$ it gives the total power. Using the 1D gain length formula [11] $L_G=\lambda_w/4\pi\rho\sqrt{3}$, we find the full width is $(1/N_w)\sqrt{L_w3/4\pi L_G}\cong(1/N_w)\sqrt{L_w/4L_G}$. This width is narrower than $2/N_w$ as long as $L_w<16L_G$. So when the wiggler length is much shorter than 16 power gain lengths, if we choose n_l to be equal to the number of periods N_w, to good approximation there is only one line within the bandwidth centered around the resonant frequency. Therefore when the wiggler length is much shorter than 16 power gain lengths TDA3D serves as a good approximation to the output power even though it handles only one single spectral line, and does not provide all the information about the spectrum.

Next, we shall explain why we can use only a small number of simulation particles to study the SASE effect while the actual number of electrons is many orders of magnitude more than a computer memory can handle. In the following, we shall show that during the exponential growth before saturation, the average output power is inversely proportional to the number of simulation particles in an optical wavelength. That is, we can calculate the average output power $\langle P\rangle$ using the averaged simulation output power $\langle P'\rangle$:

$$\langle P\rangle=\frac{N'_\lambda}{N_\lambda}\langle P'\rangle, \tag{2}$$

where N_λ and N'_λ are the line density of the electrons and simulation particles, respectively, or, equivalently, we choose them to be the number of electrons and simulation particles within one optical wavelength, respectively.

We would like to elaborate a little about the meaning of the ''simulation particles'' here. On the right hand side of the Maxwell equation, the simulation particles used in TDA behave like macro particles, each carrying charge much larger than the actual electron, so that their density distribution provides an average charge density equal to the actual charge density. However, in Newton's equations of motion, they follow the same motion as if they are actual electrons each with the same charge as a single electron. Therefore this concept of ''simulation particle'' is a mathematical abstrac-

tion, which is unphysical but useful in the calculation. The more quantitative meaning of this concept will become clear during the following derivation of the scaling relation.

Before deriving this result for a special case when the angular divergence and energy spread of the electron beam are zero, we point out that this conclusion has been verified for many cases with finite energy spread and emittance by direct simulation after averaging over many runs with different initial random electron distributions.

To derive the scaling relation of output power with the number of simulation particles, we first write down the Maxwell equation in the form used in the code TDA [12]:

$$\left(\frac{\partial}{\partial z}+\frac{1}{2ik_s}\nabla_\perp^2\right)a_s e^{i\phi_s}=i\frac{eZ_0}{mc^2}\frac{[JJ]}{2k_s}\frac{I_0}{N_\lambda}\sum_{j=1}^{N_\lambda}\delta(x-x_j)\times\delta(y-y_j)a_w(x_j,y_j)\frac{e^{-i\theta_j}}{\gamma_j}, \tag{3}$$

where $a_s e^{i\phi_s}$ is the dimensionless slowly varying amplitude and phase of the radiation signal, a_w is the wiggler's dimensionless vector potential, k_s the wave number of the radiation, I_0 the beam current, θ_j is the ponderomotive phase of the electron j, γ_j the energy of the electron j, $Z_0=377\ \Omega$ the vacuum impedance, and $[JJ]$ the Bessel factor. We would like to apologize here for the possible confusion due to the mixed notations introduced from the two references [2,12]; we used notations from both references because it is essential we compare the equations in these two references to derive the scaling relation. We emphasize that during the derivation of Eq. (3) from the Maxwell equation, with a careful examination, we found that if the sum is over the number of electrons N_λ within a certain longitudinal distance, such as over a ponderomotive period λ_r in the example here, the current I_0 has to be also divided by N_λ as shown on the right hand side of Eq. (3). If we increase the distance to n_l periods, i.e., sum over n_l cells, the denominator should be replaced by $n_l N_\lambda$. However, in actual calculation, this number must be replaced by a much smaller number N'_λ, the number of simulation particles. In TDA, the Maxwell equation (3) is coupled with the equations of motion of the simulation particles. As we move along the wiggler by increasing z in one step, the code uses the field value and the dynamic variables of the simulation particles to trace the new values at the next step, using these equations. We emphasize that in the TDA code, when we replace N_λ by N'_λ, all the other parameters such as the current I_0 are kept the same, so the only changes are to replace $(1/N_\lambda)\Sigma_{j=1}^{N_\lambda}$ by $(1/N'_\lambda)\Sigma_{j=1}^{N'_\lambda}$ in the Maxwell equation and to trace N'_λ equations of motion of the particles instead of N_λ. We shall show now that this replacement will not change the growth rate, but will increase the shot noise inversely proportional to N'_λ.

In Ref. [2] we derived the start-up noise by the coupled Maxwell and Vlasov equations. The Maxwell equation corresponding to Eq. (3) is written in the form [see Eq. (2.23) of Ref. [2]]

$$\left(\frac{\partial}{\partial\tau}+\frac{\partial}{\partial\zeta}-i\nabla_\perp^2\right)E=D_1 e^{-i\zeta}\int\frac{d\gamma}{\gamma}f, \tag{4}$$

where $\tau=k_w z$, and, as in Ref. [2], we use ζ to represent the ponderomotive phase (while in TDA [12] θ is used). E is the slowly varying amplitude and phase of the electric field, corresponding to $a_s e^{i\phi_s}$ of Eq. (3) of TDA. f is the electron distribution function normalized so that $n_0\int f d\gamma$ is the electron density, where n_0 is the peak electron density. Notice that the definition of the transverse Laplacian $\nabla_\perp^2$ in Ref. [2] is different from that in Eq. (3): the transverse coordinates are scaled as

$$\vec{\mathrm{x}}=\sqrt{2k_s k_w}\vec{\mathrm{r}}, \tag{5}$$

as defined by Eq. (2.20) of Ref. [2]. D_1 is a constant given by

$$D_1=\frac{\mu_0 n_0 e^2 c A_w[JJ]}{2mk_w}, \tag{6}$$

where A_w is the maximum value of the vector potential of the wiggler magnetic field, μ_0 the vacuum permeability. For a helical wiggler, replacing $[JJ]$ by 1 in D_1, this becomes identical to Eq. (2.25) of Ref. [2].

The Vlasov equation is [see Eq. (2.24) of Ref. [2] and the explanation following it]

$$\frac{\partial f}{\partial\tau}+\eta\frac{\partial f}{\partial\zeta}=D_2 E e^{i\zeta}\frac{1}{\gamma}\frac{\partial f_0}{\partial\gamma}, \tag{7}$$

where $\eta=1-\gamma_0^2/\gamma^2$ is the energy deviation from the resonant energy, and D_2 is given by [for helical wiggler, replace $[JJ]$ by 2, not 1, as seen from Eq. (2.26) of Ref. [2]]

$$D_2=\frac{e^2 A_w[JJ]}{4m^2c^3k_w}, \tag{8}$$

and f_0 is the smoothed undisturbed initial distribution function Eq. (2.21) of Ref. [2]:

$$f_0=u(\zeta,\mathbf{x})\delta(\gamma-\gamma_0), \tag{9}$$

where u is the transverse profile. For a step-function profile, it is simply the step function. In Ref. [2] the Maxwell equation [Eq. (4)] and the Vlasov equation [Eq. (7)] are coupled to eliminate the distribution function f, resulting in a third order partial differential equation, the envelope equation for the electric field [Eq. (2.39) of Ref. [2]]:

$$\frac{\partial^2}{\partial\tau^2}\left(\frac{\partial}{\partial\tau}+\frac{\partial}{\partial\zeta}-i\nabla_\perp^2\right)E=(2\rho)^3\left(\frac{\partial}{\partial\tau}+\frac{\partial}{\partial\zeta}+i\right)uE, \tag{10}$$

where the Pierce parameter [11], as we mentioned before, is given by $(2\rho)^3=2D_1D_2/\gamma_0^3$. This is a homogeneous equation, and its Green function and hence the growth rate of the system are determined by the Pierce parameter ρ and the profile function u. The solution of this envelope equation is obtained from the Green function and the initial conditions. In the special case of SASE, the initial condition is set by the initial distribution function f.

The main point now is the observation that the term $e^{-i\zeta}\int f d\gamma$ in Eq. (4) corresponds to the sum

$(1/N_\lambda)\sum_{j=1}^{N_\lambda} e^{-i\theta_j}$ in TDA code [Eq. (3)]. When the sum $(1/N_\lambda)\sum_{j=1}^{N_\lambda}$ in TDA is replaced by $(1/N'_\lambda)\sum_{j=1}^{N'_\lambda}$, the constants in front of the sum in Eq. (3) are not changed. In particular, the current I_0 is not changed. In the Maxwell-Vlasov equation analytical approach, this replacement corresponds to a replacement of the particle density n_0 in the term $e^{-i\zeta}\int f d\gamma$ in Eq. (4) by

$$n'_0 = \frac{N'_\lambda}{N_\lambda} n_0 . \tag{11}$$

However, in Eq. (4), the constant D_1 in front of $e^{-i\zeta}\int f d\gamma$ is not changed, i.e., the density n_0 in the expression of D_1 in Eq. (6) is not replaced by n'_0.

In the derivation of start-up from shot noise in Ref. [2] we used the initial distribution [see Eq. (5.3) of Ref. [2]]

$$f(\tau=0) = \frac{1}{n_0}\sum \delta(z-z_j)\,\delta(\mathbf{r}-\mathbf{r}_j)\,\delta(\gamma-\gamma_0). \tag{12}$$

The replacement of N_λ by N'_λ in TDA3D corresponds to replacing n_0 in this initial condition by n'_0, as given in Eq. (11). Similarly in the Vlasov equation (7), the only change is the density of the distribution f, the constant D_2, and the smoothed distribution function f_0, and hence the profile function u is not changed. Because when we replace the density n_0 of the function f by n'_0, the constants D_1, D_2 and the beam transverse profile u in the coupled Maxwell-Vlasov equation are not changed, and during the derivation of the envelope equation [Eq. (10)] the function f is eliminated, the resulting envelope equation is left unchanged. Therefore the replacement of N_λ by N'_λ in TDA3D does not correspond to a change in the envelope equation (10). Therefore the growth rate and Green function of the system remain unchanged.

It is clear from this discussion that only the initial condition is changed, and the growth rate and Green function of the system do not change. Based on this analysis, we have traced step by step the shot noise derivation of Ref. [2] [from Eq. (5.1) to Eq. (5.16) of Sec. V of Ref. [2]], to make sure that the parameter n_0 associated with the initial condition f, Eq. (12), always be replaced by n'_0, but the same parameter n_0 that appeared in D_1 does not change. The derivation is straightforward but tedious, as described in detail in Sec. V of Ref. [2], so we shall not duplicate it, but only give a brief description here. The basic idea of the derivation is that the contribution to the radiation field from each particle starts from a δ function determined by the initial distribution Eq. (12), then evolves during the FEL interaction according to the Green function $\dot{g}$ [Eq. (4.10) of Ref. [2]], determined by the coupled Maxwell-Vlasov equations. The output field is then a sum of these contributions. Therefore the replacement of N_λ by N'_λ in TDA3D corresponds to the replacement of Σ by Σ' in our analytical derivation, where the prime in the sum indicates that the sum is over a random distribution with density n'_0 instead of n_0. Thus, for example, the electric field E is given [see Eq. (5.8) of Ref. [2]] by

$$E(\tau,\zeta,\vec{\mathrm{x}}) = \frac{b\kappa}{n'_0}\sum{}' e^{-i\zeta_j}\dot{g}(\tau,\zeta-\zeta_j,\vec{\mathrm{x}},\vec{\mathrm{x}}_j). \tag{13}$$

This can be obtained simply by replacing each δ function in the initial condition Eq. (12) by the corresponding Green function $\dot{g}$ with a corresponding phase factor, replacing $(1/N_\lambda)\sum_{j=1}^{N_\lambda}$ by $(1/N'_\lambda)\sum_{j=1}^{N'_\lambda}$, and then multiplying by a constant. For simplicity, we shall not quote the constants b, κ and the Green function $\dot{g}$ here, and only refer to Eqs. (5.5), (5.6), and (4.2), (4.13) of Ref. [2], because they are not essential for our conclusion about the scaling relation here. We only emphasize that the density n_0 found in κ of Eq. (5.6) of Ref. [2] remains to be n_0, not to be replaced by n'_0. $\vec{\mathrm{x}}$ is the scaled transverse position given by Eq. (5). Finally, using the electric field Eq. (13), and the fact that the density in the sum Σ' is n'_0 instead of n_0, we find the output power [see Eqs. (5.10), (5.14), and (5.15b) of Ref. [2]]

$$\langle P'\rangle = \frac{k_s\kappa^2}{Z_0 n'_0}\int d^2x \int d^2x_1 \int d\zeta |\dot{g}(\zeta-\zeta_1,\vec{\mathrm{x}},\vec{\mathrm{x}}_1)|^2 u(\vec{\mathrm{x}}_1).$$

The only difference of this result from Ref. [2] is the replacement of n_0 by n'_0. Hence, using this equation and the relation Eq. (11) between n_0 and n'_0, we immediately find the scaling result

$$\langle P\rangle = \frac{N'_\lambda}{N_\lambda}\langle P'\rangle .$$

This scaling relation and the discussion about how to use the single frequency code to calculate output power make it possible for us to calculate the SASE power by TDA3D.

III. THE ANALYTICAL ESTIMATE

To test the simulation, we need an analytical estimate. Our analytical estimate for start-up noise is based on a 3D theory [2,3] for an electron beam with a step-function profile, zero energy spread, and zero angular spread. We use this idealized model here because this problem has been solved explicitly. We apply the newly developed simulation method to the same case, to check the accuracy of the simulation. In addition, as a by-product, we found that this idealized model can be used for estimating the start-up noise of the 1 μm SASE experiment at ATF of BNL [1]. The geometrical emittance in this case is much smaller than the wavelength divided by 2π, and the betatron wavelength (3 m) is much longer than two power gain lengths ($\sim$0.2 m), resulting in negligible betatron motion during the start-up process. If we choose the beam radius such that it has the same rms beam size and same current, then the model has a growth rate quite close to that of the more realistic waterbag model. In Sec. IV, we shall see that when we choose this idealized set of parameters, the analytical estimate agrees very well with the simulation results, providing support for the validity of the simulation.

Based on the analysis of Refs. [2,3], the ratio of SASE radiation spectrum in the guided mode n over spontaneous radiation spectrum is given by

$$\frac{(dP_{nn}/d\omega)_{\mathrm{SASE}}}{(dP/d\omega)^{L_w}_{\mathrm{spon}}} = \frac{1}{9}e^{L_w/L_{G_n}}C_n(\tilde{a})\frac{2L_{G_n}}{L_w}, \tag{14}$$

where L_w is the wiggler length, and P_{nn} and L_{G_n} are the output power and the power gain length in the guided mode n, respectively. The label n used here actually represents an index, which could be a set of several discrete indexes. For example, it could be $\{j,m\}$, where m is the azimuthal node number and j the radial node number. So the notation ''n'' should be understood as appropriate for the text where it appears. As explained in [2], the power is a sum over ''diagonal'' terms P_{nn} and ''cross'' terms P_{nl}, and the cross terms P_{nl} are usually negligible. So the measured ratio is the sum over all the modes. The factor $C_n(\tilde{a})$ is the coupling of the radiation from the first two power gain lengths into the guided mode n. We shall describe the calculation of this factor briefly in the following and then present it in detail in the Appendix.

The meaning of this formula is very clear: the factor $2L_{G_n}/L_w$ multiplied by the spontaneous power spectrum $(dP/d\omega)^{L_w}_{\text{spon}}$ is the power spectrum of the first two power gain lengths (one field gain length). This is then multiplied by a coupling factor $C_n(\tilde{a})$, representing the equivalent start-up noise as an equivalent input seed, to be amplified by a factor $\frac{1}{9}e^{L_w/L_{G_n}}$, where the factor $\frac{1}{9}$ represents the well known lethargy distance for an input signal to be amplified before reaching an exponential growth in a 1D theory.

The gain length L_{G_n} and the coupling factor $C_n(\tilde{a})$ can be calculated, once the scaled beam size $\tilde{a}$ is given, which is defined by Eq. (6.13) of Ref. [2] as $\tilde{a}=\sqrt{2\rho}\sqrt{2k_wk_s}R_0$, where k_w, k_s are the wiggler and radiation wave number, respectively; R_0 the radius of the step profile; and ρ the Pierce parameter. The growth rate per wiggler period in 1D theory, given already following Eq. (10) in Sec. I, is also defined following Eq. (5) of [13]:

$$(2\rho)^3=\frac{n_0Z_0e^2K_{\text{rms}}^2[JJ]^2}{2m\gamma^3k_w^2c}, \tag{15}$$

with K_{rms} the rms wiggler parameter, which is represented in TDA as a_w in the previous Eq. (3). For helical wiggler, $[JJ]$ in the expression for ρ in Eq. (15) is replaced by 1.

From Refs. [2,3], it follows that the coupling factor is given by

$$C_n(\tilde{a})=\left(\frac{2}{\pi\tilde{a}^2}\frac{\text{Im}(\lambda_n)}{|\lambda_n|^2}N_{nn}\frac{9}{|F_n|^2}\right). \tag{16}$$

The variables λ_n, N_{nn}, and F_n for a mode n are calculated as explained in detail in the Appendix, through three variables ϕ and χ and the scaled growth rate λ, which for each mode n are calculated in turn by solving the set of three coupled equations (6.14), (6.15), (6.16) of [2], once the scaled beam size $\tilde{a}$ is given and the detuning $\Delta=\Delta\omega/\omega$ is assumed to be zero.

Once the scaled growth rate λ_n is known, the power gain length is given by

$$L_{G_n}=\frac{\lambda_w}{8\pi\rho\ \text{Im}(\lambda_n)}, \tag{17}$$

where λ_w is the wiggler period.

The variables N_{nn} and F_n in the parentheses are then calculated by Eqs. (6.31) and (6.30) of [2], respectively. These expressions are complicated but the calculation is straightforward and is given in the Appendix. To a good approximation, when $\tilde{a}>0.25$ the calculated results for $C_n(\tilde{a})$ and $\text{Im}(\lambda_n)$ as functions of $\tilde{a}$ are fit with

$$\text{Im}(\lambda_n)\cong\frac{\sqrt{3}}{2}e^{-(1/\tilde{a}\sqrt{1+\tilde{a}^2})(\alpha_0+\alpha_1\,1/\tilde{a}^2)}, \tag{18}$$

$$C_n(\tilde{a})\cong\frac{\sqrt{3}}{\pi\tilde{a}^2}e^{-(1/\tilde{a}\sqrt{1+\tilde{a}^2})(\beta_0+\beta_1\,1/\tilde{a}^2)}, \tag{19}$$

where for the mode $\{1,0\}$, we have $\alpha_0=0.397$, $\alpha_1=-0.0067$, $\beta_0=1.093$, $\beta_1=-0.02$; while for the mode $\{1,\pm1\}$ we have $\alpha_0=1.2625$, $\alpha_1=-0.1494$, $\beta_0=5.082$, $\beta_1=-0.5707$.

As an example for the calculation of the ratio of SASE over the spontaneous radiation, we choose a set of parameters which give the growth rate and output power very close to the data we used to fit the the ATF SASE experimental data. We found that as long as we take the same rms beam size, the same current, and the same wiggler, the step-function profile model and the waterbag model have nearly equal growth rates. The difference for the waterbag model and the Gaussian model is also negligible for our case.

The parameters we used are given in Table I. Based on these parameters, we found the coupling into the fundamental mode $\{1,0\}$, as described in detail in the Appendix, to be 0.186, the scaled growth rate $\text{Im}(\lambda_n)=0.6915$, and the gain length is 0.111 m, hence the SASE over spontaneous radiation ratio, according to Eq. (14), is

$$\frac{1}{9}\ e^{0.534/0.111}\times0.186\times\frac{2\times0.111}{0.534}=1.06.$$

The increment due to the amplification is

$$\left(\frac{1}{9}\ e^{0.534/0.111}-1\right)\times0.186\times\frac{2\times0.111}{0.534}=0.98.$$

Similarly, the increment for the mode $\{1,\pm1\}$ is

$$2\times\left(\frac{1}{9}\ e^{0.534/0.16}-1\right)\times0.0317\times\frac{2\times0.16}{0.534}=0.08.$$

The extra factor 2 is due to the two modes with $m=\pm1$. For higher modes, the gain factor $\frac{1}{9}e^{L_w/L_{G_n}}$ is rapidly reduced to nearly one or even smaller than one, and the formula Eq. (14) is not valid. However, the gain for these higher modes is negligible; this means that they only contribute to the spontaneous radiation, so $(\frac{1}{9}e^{L_w/L_{G_n}}-1)$ for these modes can simply be replaced by 0 as an approximation.

Notice that when there is no gain, the SASE over spontaneous radiation ratio is just 1. Therefore the increment to the ratio, summing over the contributions from different modes, becomes

TABLE I. FEL Parameters used in the calculation.

	Notation	Waterbag	Step function
Electron beam energy	γ	68.49	68.49
Normalized rms emittance (mm mrad)	ϵ_n	0.7	0.7
rms energy spread	σ_γ	4.35×10^{-4}	4.35×10^{-4}
Total current (A)	I_0	320	320
Wiggler parameter (max)	$K_{\max}$	0.364	0.364
Maximum magnetic field	B_w	0.443	0.443
Wiggler length (m)	L_w	0.534	0.534
Wiggler period (cm)	λ_w	0.088	0.088
e-beam edge radius (μm)	R_0	170	138
Radiation wavelength (μm)	λ_s	1.0025	1.0000
Betatron wavelength (m)	λ_β	2.96	∞
Pierce parameter	ρ	5.04×10^{-3}	4.59×10^{-3}
Scaled beam size	$\tilde{a}$	1.61	1.25
Scaled transevese current	D	1.62×10^{-2}	
Power e-folding length (m)	L_w	0.112	0.110
Bessel factor $[JJ]$		0.984	0.984
Scaled growth rate mode $n=\{0,1\}$	$\mathrm{Im}(\lambda_{\{0,1\}})$	0.6214	0.6915
Scaled growth rate mode $n=\{\pm1,1\}$	$\mathrm{Im}(\lambda_{\{\pm1,1\}})$		0.4774

$$\frac{(dP/d\omega)_{\mathrm{SASE}}}{(dP/d\omega)^{L_w}_{\mathrm{spon}}}-1=\left(\frac{1}{9}\,e^{0.534/0.111}-1\right)\times0.186\times\frac{2\times0.111}{0.534}+2\times\left(\frac{1}{9}\,e^{0.534/0.16}-1\right)\times0.0317\times\frac{2\times0.16}{0.534}+\cdots=0.98+0.08+\cdots=1.06+\cdots\approx1.1. \tag{20}$$

Hence we found the ratio to be $1+1.1=2.1$.

The calculation shows that the higher modes only contribute to the spontaneous radiation, which in this particular case comprise half of the output power. The other half is the SASE power, which mostly comes from the fundamental mode, since the contribution from the mode $n=\{\pm1,1\}$ is much smaller. Thus the result also provides clear information about the transverse coherence of the output: it is not completely coherent yet because half of the output is due to spontaneous radiation.

IV. NUMERICAL SIMULATIONS

We now apply the result of Sec. II to check the analytical calculation of Sec. III. For example, we know that 1200 simulation particles per cell are sufficient to give the correct gain length $L_G=0.11$ m. For the idealized case of Sec. III with current of 320 A and emittance of 0.7 mm mrad, we choose the number of cells to be 61 because there are 61 periods in the wiggler, and randomly fill each cell with 1200 simulation particles. The azimuthal modes used in the calculation are from $m=-2$ to $m=2$, i.e., five modes are used. To simulate our idealized case of Sec. III, a minor modification is incorporated into the TDA3D code to provide an initial distribution with parallel electron beam and step-function profile. The focusing parameter in the code is turned off so that there is no betatron oscillation in the wiggler and the beam profile is kept constant.

The number of electrons within $\lambda_r=1\,\mu$m is $I_0\lambda_r/ec=6.7\times10^6$, so the output power 1.2×10^4 W, as given by TDA3D, is multiplied by $1200/(6.7\times10^6)$ to get the corrected simulation power of 2.2 W. Notice that in TDA the output is given in the form of gain instead of power, so we must set up an input radiation power. In our case, we set it to be 10^{-10} W, which is so small that it does not affect the output power. Using this method, varying the current from 0 to 320 A, we plot the output power as a function of current in Fig. 2, each point being an average over 30 runs. The reason that we choose to average over 30 runs, in addition to the practical consideration about our finite CPU time, is due to a consideration based on our analytical theory about intensity fluctuation [14], to be explained later in this section. Without

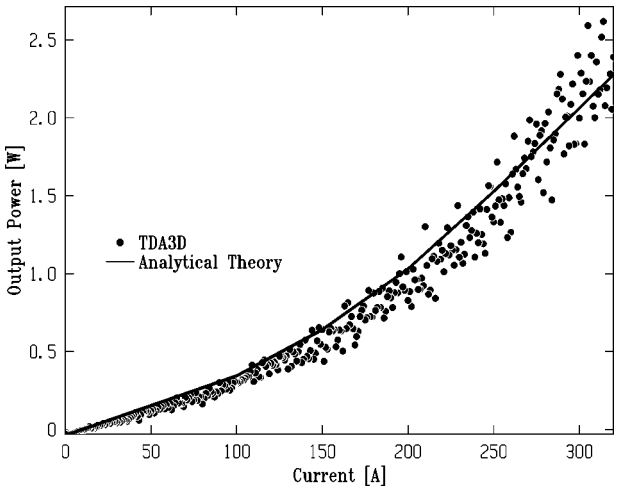

FIG. 2. Output power vs current for the step-function model.

averaging, the relative rms fluctuation would have been 100%. With an averaging over 30 runs, the resulting fluctuation mimics the observed experimental fluctuation, to be discussed later. The result shows that the power linearly increases with the current until about 100 ampere, corresponding to spontaneous radiation, and deviates from linear dependence when larger than 100 A. At 320 A, the power is a factor 2.2 larger than the linear extrapolation from the spontaneous regime. The extrapolated spontaneous power is 1.0 W.

The power of the spontaneous radiation serves as a very reliable check of the new simulation method. The spontaneous radiation power spectrum in a unit solid angle in forward direction and at the resonant frequency is given by [15]

$$B_0 \equiv \left(\frac{\partial^2 P_{\text{spont}}}{(\partial\omega/\omega)\,\partial\Omega} \right)_{\theta=0\ \omega=\omega_s} = \frac{e_0 Z_0 I_0}{4\pi} N_w^2 \gamma^2 \frac{K_{\max}^2}{(1+K_{\max}^2/2)^2} [JJ]^2 \omega = 5.7\times 10^6 \ \text{W}. \tag{21}$$

Within a bandwidth $1/N_w$ the radiation opening angle is

$$\theta_w \equiv \sqrt{\frac{2\lambda_s}{L_w}} = 1.93 \ \text{mrad}. \tag{22}$$

This opening angle has been defined in such a way that the power spectrum integrated over the full solid angle is

$$\left(\frac{dP_{\text{spont}}}{d\omega/\omega} \right)_{\text{peak}} = \pi \theta_w^2 B_0 = 67 \ \text{W}. \tag{23}$$

This peak of the power spectrum is detuned at a slightly lower frequency ω from the resonant frequency ω_s. The full bandwidth of the radiation as we mentioned in Sec. II, for the spontaneous radiation is $1/N_w$, the same as the line spacing we mentioned also in Sec. II. Thus the spontaneous radiation power within this bandwidth and solid angle is

$$\left(\frac{dP_{\text{spont}}}{d\omega/\omega} \right)_{\text{peak}} \frac{1}{N_w} = 67 \frac{1}{61} = 1.1 \ \text{W}. \tag{24}$$

This power is also called the power in the central cone. Thus we found that it agrees with the simulation to within 10%. This is an excellent agreement, considering the approximate nature of the simulation and the limited number of modes and simulation particles used.

Notice that the factor 2.2 also agrees with the previous analytically estimated value of 2.1 given by Eq. (2.2) excellently, supporting both the simulation and the approximation made in applying the analytical theory. In Fig. 2 we also plot the analytical calculation based on the description of Sec. III, with the calculated ratio multiplied by the calculated spontaneous power in the central cone (which is 1.1 W for 320 A, as mentioned above). It shows again an excellent agreement. Similar calculations have been done for various currents and emittances, and for wiggler lengths from $6L_G$ to $10L_G$, and the results always agree with the analytical estimate. We found that when we increase the number of modes and correspondingly the number of simulation particles to maintain the correct growth rate, the spontaneous radiation power increases. When we examine Fig. 2, we can see that the simulated spontaneous power is slightly lower than the theory. This is evident particularly when the current is lower than 100 A. So there will be a better agreement between the spontaneous radiation theory and the simulation, if we can further increase the number of modes. However, due to our limited CPU time, we limited the number of modes to 5 and the number of particles per cell to 1200.

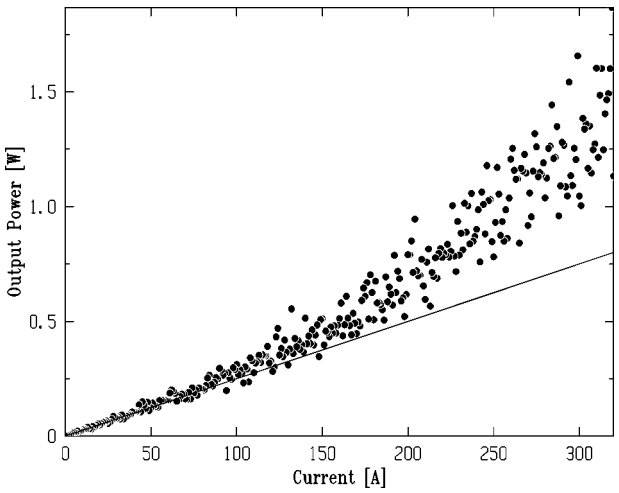

FIG. 3. Output power vs current for the waterbag model.

As we pointed out before, we have used a set of parameters very close to the 1 μm ATF SASE experiment in the idealized model. Now that we have confirmed the validity of the simulation method, to compare with the experiment more closely, we change to the more realistic waterbag model. The parameters for the waterbag model are listed in Table I together with the step-function model of Sec. III. The wiggler parameters and the betatron wavelength are based on the actual experiment, the beam current is the peak current measured by slice measurement method [16]. The local energy spread should be smaller than the experimental resolution, we take it to be 4.0×10^{-3}. However, the emittance was chosen, based on the analysis of Sec. III, to be 0.7 mm mrad to fit the observed SASE power over spontaneous power ratio, rather than the measured slice emittance of 1.4 mm mrad. We use the universal scaling function [13,17] to calculate the gain length, and compare with the simulation to find the proper number of simulation particles. Since the wiggler is much shorter than the measured betatron wavelength (3 m), even though there is no horizontal focusing, we can approximately assume the beam size as constant, and apply this formula. Because the focusing is different from the natural focusing of the wiggler, the gain length of 0.112 m is calculated using the formula given in [17] instead of the formula in [13], which is adequate for natural focusing while the formula in Ref. [17] is more general and is also valid when the focusing is different from natural focusing. The result is given in Fig. 3, which is very similar to the idealized model. This means that our analytical calculation using the idealized model provides a very convenient tool to check the simulation and analyze the experiment, as long as we use the same wiggler, the same beam current, and the same rms beam size.

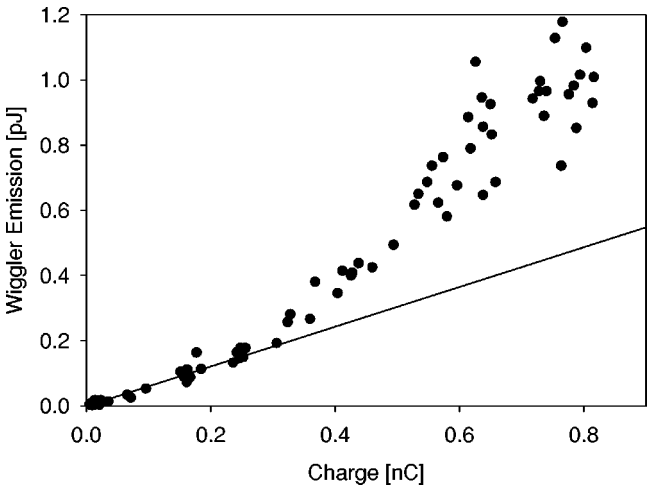

FIG. 4. Output pulse energy vs charge of the ATF experiment.

As a minor detail, notice that to have the same rms beam size, the edge radius of the step-function model should be $R_{\text{step}}=2\sigma_x=\sqrt{\frac{2}{3}}R_{\text{water}}=138\ \mu$m, where σ_x is the rms beam size and R_{water} the edge beam size for the waterbag model. Also notice that because the Pierce parameter ρ is slightly different for the step-function model and the waterbag model, the scaled beam sizes for the two models are related by $\tilde{a}_{\text{step}}=(\frac{2}{9})^{1/6}\tilde{a}_{\text{water}}=1.25$.

For a comparison, the ATF experimental data [18] are plotted in Fig. 4, showing the pulse energy as a function of the electron bunch charge. The measurement has a bandwidth of 25 nm, corresponding to a relative bandwidth of 25 nm/1 μm=1/40. The opening angle is 1.2 mrad, which is smaller than the opening angle of the radiation for a fixed frequency given by Eq. (22), i.e., 1.9 mrad. Hence within this observation angle, the bandwidth is $1/N_w=1/60<1/40$. Therefore the bandwidth is not reduced by the measurement, but the solid angle is reduced by a factor $(1.2/1.9)^2=0.4$. The spontaneous radiation power, according to our calculation, should be $1.1\times0.4=0.44$ W. To calculate the pulse energy, we use the width of the central part of the measured pulse, about 2 ps, because most of the SASE energy comes from the peak part, and from the slice measurement [16] we get 2 ps. So the pulse energy is estimated to be $0.44\times2\times1.9=1.6$ pJ. The ratio 1.9 is taken from Fig. 3. In Fig. 3 the simulation gives 0.8 W as the spontaneous radiation power, but we use the calculated 1.1 W instead; this is because we know that when we increase the number of modes, the result approaches the correct value of 1.1 W, while we found that the ratio of 1.9 is insensitive to the number of modes. The measured pulse energy at the maximum charge, corresponding to 320 A of peak current, is calibrated to be 1.1 pJ. Taking into account the approximate nature of all these estimates, this is a reasonable agreement.

To further check the new simulation method for SASE, we compared with the result of a run using the time-dependent code GINGER, provided by Fawley [8]. The result is consistent with the GINGER calculation, but we cannot claim a rigorous confirmation, because the random nature of the SASE output requires a much larger number of runs of the code GINGER to give sufficient statistics.

The analytical analysis shows that to achieve the experimental finding of the ratio 1.9 of the SASE pulse energy over the spontaneous radiation, the emittance should be 0.7 mm mrad. The result is very sensitive to the emittance. For example, if the emittance increases to 1 mm mrad, the ratio drops to 1.5. The measured global emittance is 2.4 mm mrad, while the measured slice emittance is 1.4 mm mrad. However, this deviation from calculation is not an inconsistency because as the experimental group explained [18], the measurement could be a pessimistic one, i.e., the realistic distribution could be such that both the longitudinal and transverse tails of the phase space distribution contribute significantly to the emittance measurement, but would not have much influence on the performance of the FEL interaction. Therefore our results raise a challenge to the further improvement of the emittance measurement, or phase space distribution measurement technique, and also more detailed analysis of the effect of the phase space distribution.

Finally, we shall explain why we averaged over 30 runs for each point in Figs. 2 and 3. Recently, to explain the intensity fluctuation in the experiment, we developed a 3D analytical theory [14], the result shows that the fluctuation is given by

$$\frac{\sigma_w}{W}=\frac{1}{\sqrt{l/l_c}}, \tag{25}$$

where σ_w is the rms fluctuation of the output SASE energy W per pulse, l is the length of a flat-top pulse, and l_c is a correlation length characterizing SASE coherence. We find

$$l_c=N_w\lambda_s\left(\frac{2\pi}{3}\frac{L_G}{L_w}\right)^{1/2}, \tag{26}$$

where N_w is the number of undulator periods, λ_s is the radiation wavelength, L_w the undulator length, and L_G is the power e-folding length.

In the recent BNL ATF SASE experiment the gain length is about 0.11 m according to our analysis, i.e., the wiggler has 4.9 gain length, 60 periods. So the slippage is 60 μm, and the coherence length is reduced to $60\ \mu\text{m}/\sqrt{3/2\pi\times4.9}=40\ \mu$m. The pulse length is measured to be about 4 ps, i.e., about 1300 μm, so the number of coherence length in the electron bunch is $1300\ \mu\text{m}/40\ \mu\text{m}\approx30$. The SASE theory told us that the output can be approximated by the sum of 30 independently evolved spikes in the single bunch. Therefore, to simulate the fluctuation we averaged over 30 runs to give each point in Figs. 2 and 3. The fluctuation $\sigma_w/\langle W\rangle$ is calculated to be about $\sqrt{40/1300}\cong17\%$. This is consistent with the measured fluctuation of about 15%, considering that the pulse shape is actually not a step function and the calculated beam size is not really large enough to be near the 1D limit.

V. CONCLUSION

We have developed two very different methods to calculate the SASE output power: the numerical simulation of TDA3D using the scaling relation, and the analytical method. The two methods agree with each other very well. The calculation has been used to analyze the recent ATF 1 μm SASE experiment. Since the scaled beam size $\tilde{a}$ is of order

one, the case is clearly a three-dimensional case, a 1D analysis is not appropriate. Our new methods of three-dimensional calculation provide a very useful tool to analyze the recent SASE experiments.

We provide a very detailed description of the calculation in the hope that a reader should be able to apply the methods to carry out the calculation of SASE without going through the detailed derivation in the previous papers [2,3]. However, we also provide detailed references to our previous works so that a reader, who is interested in the details of the derivation, can follow it step by step.

ACKNOWLEDGMENTS

The author would like to thank Dr. S. Krinsky for many discussions and suggestions. The author also thanks Dr. I. Ben-Zvi for many discussions on the recent SASE experiment at ATF, and his many suggestions. We would also like to thank Dr. W. Fawley for providing the simulation results from GINGER to test our new simulation approach. This work was performed under the auspices of the U.S. Department of Energy.

APPENDIX: CALCULATION DETAILS FOR THE GUIDED MODES

As explained in [2], to calculate the coupling coefficients, given the scaled beam size $\tilde{a}$, we first solve the following coupled equations for the three variables χ, ϕ, and λ for a mode specified by $n=\{m,j\}$, with an azimuthal node number m, and a radial node number j, using Newton's root finding routine. Using a software such as Mathematica, the calculation is not much more than copying the following equations, and then using the command ''FindRoot'' in a mathematical calculation:

$$\chi\frac{J_m'(\chi)}{J_m(\chi)}=\phi\frac{H_m^{(1)'}(\phi)}{H_m^{(1)}(\phi)},$$

$$\phi^2-\chi^2=\frac{\tilde{a}^2}{\lambda^2}\left(1-2\rho\frac{\phi^2}{\tilde{a}^2}\right)\cong\frac{\tilde{a}^2}{\lambda^2},$$

$$\lambda=\frac{\phi^2}{\tilde{a}^2}+\Delta,$$

where $J_m(\chi)$, $H_m^{(1)}(\phi)$ are Bessel function and Hankel function, respectively, λ is the scaled growth rate, and Δ is the scaled detuning, taken to be zero for our case. The mode number n is determined by the initial trial value of the solution, which is known for large $\tilde{a}$. The solution for smaller $\tilde{a}$ is obtained by gradually reducing $\tilde{a}$, using the previous solution for slightly larger $\tilde{a}$ as trial solution. Notice that the second equation [Eq. (6.14) of [2]] is simplified as compared with Ref. [2] because ρ is very small.

Then N_{nn}, F_n are calculated by

$$N_{nn}=4\frac{(\xi-\xi^*)^2}{\xi^2\xi^{*2}}\frac{(\chi\chi^*)^2}{[\tilde{a}(\chi^2-\chi^{*2})]^2}\frac{(\phi\phi^*)^2}{\phi^2-\phi^{*2}}(\lambda^{*2}-\lambda^2),$$

$$F_n=-\frac{\phi^2}{\phi^2-\chi^2}\left(1+\frac{\chi^2}{\xi^2}\right)\frac{2}{\lambda^3},$$

with

$$\xi\equiv\chi\frac{J_m'(\chi)}{J_m(\chi)}.$$

Even though these expressions seem rather complicated, their physical meaning is clarified in [3] for large and small beam size limit, i.e., for $\tilde{a}\gg 1$, or $\tilde{a}\ll 1$.

[1] An incomplete list of the recent SASE experiments: R. Prazeres *et al.*, Phys. Rev. Lett. **78**, 2124 (1997); M. Hogan *et al.*, *ibid.* **80**, 289 (1998); R. L. Schefield, J. C. Goldstein, and D. C. Nguyen, in *Free Electron Laser Challenges*, SPIE Proceedings Vol. 2998, edited by P. O'Shea (The International Society for Optical Engineering, San Jose, CA, 1997); M. Babzien *et al.*, Phys. Rev. E **57**, 6093 (1998).

[2] S. Krinsky and L. H. Yu, Phys. Rev. A **35**, 3406 (1987).

[3] L. H. Yu and S. Krinsky, Nucl. Instrum. Methods Phys. Res. A **285**, 119 (1989).

[4] J. M. Wang and L. H. Yu, Nucl. Instrum. Methods Phys. Res. A **250**, 484 (1986).

[5] K. J. Kim, Nucl. Instrum. Methods Phys. Res. A **250**, 396 (1986).

[6] K. J. Kim, Phys. Rev. Lett. **57**, 1871 (1986).

[7] K. J. Kim, Nucl. Instrum. Methods Phys. Res. A **393**, 167 (1997).

[8] W. Fawley, A. M. Sessler, and E. T. Scharlemann, Bull. Am. Phys. Soc. **38**, 1327 (1993); W. Fawley, Report No. LBID-2141, CBP Tech Note-104, UC-414, 19xx (unpublished).

[9] C. Penman and B. W. J. McNeil, Opt. Commun. **90**, 82 (1992).

[10] L. H. Yu, Phys. Rev. A **44**, 5178 (1991).

[11] R. Bonifacio, C. Pellegrini, and L. M. Narducci, Opt. Commun. **50**, 373 (1984).

[12] T. M. Tran and J. S. Wurtele, Comput. Phys. Commun. **54**, 263 (1989).

[13] L. H. Yu, S. Krinsky, and R. Gluckstern, Phys. Rev. Lett. **64**, 25 (1990); **64**, 3011 (1990).

[14] L. H. Yu and S. Krinsky, Nucl. Instrum. Methods Phys. Res. A **407**, 261 (1998).

[15] S. Krinsky, M. L. Perlman, and R. E. Watson, in *Handbook on Synchrotron Radiation*, edited by E. E. Koch (North-Holland, Amsterdam, 1983), Vol. 1.

[16] X. Qiu *et al.*, Phys. Rev. Lett. **76**, 3723 (1996).

[17] L. H. Yu, C. M. Hung, D. Li, and S. Krinsky, Phys. Rev. E **51**, 813 (1995).

[18] M. Babzien, I. Ben-Zvi, P. Catravas, J-M. Fang, Y. Liu, T. C. Marshall, X. J. Wang, J. S. Wurtele, V. Yakimenko, and L. H. Yu, Phys. Rev. E **57**, 6093 (1998).